https://doi.org/10.3311/PPtr.22671

Periodica Polytechnica Transportation Engineering, 52(1), pp. 67–74, 2024

Comparison of Different Turbulence Models and Wall Treatment Methods for Vehicle Aerodynamics Investigations

Brúnó Péter[1], István Lakatos[1*]

[1] Department of Automotive and Railway Engineering, Audi Hungaria Faculty of Automotive Engineering,
Széchenyi István University, Egyetem tér 1., H-9026 Győr, Hungary
[*] Corresponding author, e-mail: lakatos@sze.hu

Received: 28 May 2023, Accepted: 26 October 2023, Published online: 11 December 2023

Abstract

In this paper two different turbulence models and wall treatment methods were investigated with Computational Fluid Dynamics (CFD) method. The used geometry for the research was the Ahmed body. The Ahmed body is a widely used geometry in vehicle aerodynamics investigations. The geometry represents a simplified vehicle, which allows the researchers to make examinations with moderate resources. The simulations were made in Ansys Fluent. The environment of the simulation was built to optimize for maximum 8 GB RAM. The paper examines the difference between the k-ω SST and the k-ε turbulence models in the case of low and high Reynolds number wall treatment methods. This could be useful because the high Reynolds number wall treatment method needs less computational capacity based on that, its required y^+ range is between 30 and 300. While in the case of the low Reynolds wall treatment method the required y^+ range is below 10, which could increase the cell count. The results from the CFD simulation will be compared to each other and with measured data. The aim of the research is to get information about behaviour of the examined turbulence models in the case of low and high Reynolds number wall treatment methods.

Keywords

Ahmed body, Computational Fluid Dynamics, k-ω SST turbulent models, k-ε realizable turbulent models, low Re wall treatment methods, high Re wall treatment methods

1 Introduction

The history of passenger vehicles has been started at the beginning of the 20th century (Suda, 2022). The development can be divided into four main periods. The first one was the borrowed shapes period from 1900 to 1930. These vehicles had basis geometry e.g., torpedo or the boat tail geometries. The second period was the streamlining from 1921 to 1955. At this time the developers modified the shape of the bodies to get more efficient geometries from aerodynamic point of view. One of the most popular body shapes from this period is the Jaray's shape, which was developed by a Hungarian engineer and designer. The next period was the detail optimization stage, which started in 1955. At this time smaller modifications were made on the vehicles, for instance, optimization of the radiuses, changing the roof camber, inclination angles etc. The last period is the shape optimization era which started in 1983.

In the 1900s, the aerodynamics development of the vehicles was made with the help of wind tunnel measurements (Hucho, 1987). This method was not cost efficient and took a lot of time. The discipline had evolved, and the Computational Fluid Dynamics was invented around 1920. Following, the development of the vehicles' aerodynamics had been sped up (Wei, 2017). Nowadays, a lot of investigations of the vehicle aerodynamics are made with the help of Computational Fluid Dynamics (Ragheb and El-Gindy, 2022). This method is not only useful from aerodynamics point of view but the results from it could be used to improve other beneficial applications (Galipeau-Bélair et al., 2013). However, due to the complicated vehicle shapes (Székely and Ficzere, 2017), modelling the flow around it, still consumed a lot of time and cost (Veress et al., 2008).

In 1984 Ahmed and other scientists created a simplified body, which could represent a vehicle (Banga et al., 2015). This shape is called Ahmed body. The Ahmed body is a bluff body. The basis of the geometry is to get a simplified model with which the calculations could be made with high accuracy but which is similar to a vehicle to such an extent that the results could be used for road vehicle development.

Cite this article as: Péter, B., Lakatos, I. (2024) "Comparison of Different Turbulence Models and Wall Treatment Methods for Vehicle Aerodynamics Investigations", Periodica Polytechnica Transportation Engineering, 52(1), pp. 67–74. https://doi.org/10.3311/PPtr.22671

It is important because lots of vehicles are on the roads and fuel consumption / vehicles' global warming impact and drag coefficient of the vehicle are in strong connection (Vučetić et al., 2022). Therefore, low drag coefficient is essential to keep the environmental pollution at a low level, which is studied by several papers (Matijošius et al., 2022).

A lot of research has been carried out about the Ahmed body in the past. Francois Delassaux and his partners investigated flow around the Ahmed body with SST RANS and with hybrid approaches (Delassaux et al., 2021). Different slant angles of the Ahmed body were examined using time-averaged and continuous flow characteristic (Tunay et al., 2014) and Reynolds averaged, unsteady Navier-Stokes equations (Bayraktar et al., 2001). The c-pillar vortices were studied with numerical methods by M. Corallo (Corallo et al., 2015). The turbulent flow is investigated around the well-known body with LES simulations by M. Minquez. Multidomain spectral Chebyshev–Fourier solver was used by (Minguez et al., 2008). The flow separation at the hatchback is investigated with PANS turbulence model (Rao et al., 2018). Two-dimensional approach was focused on different rear windows (Bruneau et al., 2007). Different underbody constructions were studied with CFD simulations (Buscariolo et al., 2021). The wake zone after the vehicle was investigated by J. Venning (Venning et al., 2022). With the help of the Large Eddy simulation method, the near wake flow was studied (Bing-xin et al., 2019).

As mentioned before, development of the vehicles has different methods. One of these is the CFD simulation, which will used in this article (Jéger and Veress, 2019). A CFD simulation has a wide variety of settings e.g., the structure of the numerical mesh, different turbulence models or wall treatment methods. In this article two turbulence models will be examined with low and high Reynolds number wall treatment methods. The two turbulence models are the widely used *k*-omega STT in vehicle aerodynamics and the *k*-*ε* realizable with the Enhanced Wall Treatment setting.

The aim of the article is to investigate the difference between the above-mentioned turbulence models in the case of low and high Reynolds number (Re) wall treatment methods as well. Examining the high Reynolds number wall treatment method is useful because with this method a significant amount of cell count could be saved. The high Reynolds number wall treatment method is allowed to keep the y^+ value in the range of 30 to 300, which allows to set the first boundary cell's height bigger (Kristóf, 2019). While in the case of the low Reynolds number wall treatment method the correct y^+ range is below 10. The y^+ is the non-dimensional distance normal to the wall. It can be calculated as:

$$y^+ = \left(\rho \times y \times u^*\right)/\mu, \tag{1}$$

where ρ is the density of the freestream, y is the distance of the cell centroid, u^* is the friction velocity and μ is the dynamic viscosity.

2 Theoretical background

2.1 Grid Convergence Index method

The mesh convergence investigation was made by the Grid Convergence Index method (Celik et al., 2008). This method is based on the Richardson extrapolation. The aim of this investigation to obtain the relative and the discretization errors of the examined meshes. The errors could be calculated with the following equations.

First of all, the representative cell size (h) should be calculated as:

$$h = \left[\frac{1}{N}\sum_{i=1}^{N}\left(\Delta V_i\right)\right]^{1/3}. \tag{2}$$

In the case of 3D simulation where N represents the cell count and ΔV_i represents the volume. After that, the refinement factor can be obtained (Eq. (3)), which is the ratio of the representative cell size of the medium (h_{medium}) and the fine (h_{fine}) mesh. This ratio should be greater than 1.3.

$$r = \frac{h_{medium}}{h_{fine}}. \tag{3}$$

In the next step, the apparent order can be obtained as:

$$p = \frac{1}{\ln\left(r_{21}\right)}\left|\ln\left|\varepsilon_{32}/\varepsilon_{21}\right| + q\left(p\right)\right|, \tag{4}$$

where:

$$q\left(p\right) = \ln\left(r_{21}^p - s/r_{32}^p - s\right), \tag{5}$$

$$s = 1 \times sign\left(\frac{\varepsilon_{32}}{\varepsilon_{21}}\right), \tag{6}$$

$$\varepsilon_{32} = \Phi_3 - \Phi_2, \tag{7}$$

$$\varepsilon_{21} = \Phi_2 - \Phi_1. \tag{8}$$

Then, the extrapolated value, which belongs to the finite mesh, can be calculated as:

$$\Phi_{ext}^{21} = \left(r_{21}^{p} \times \Phi_1 - \Phi_2\right) / \left(r_{21}^{p} - 1\right). \tag{9}$$

Finally, the relative $\left(e_a^{21}\right)$ and the extrapolated error $\left(e_{ext}^{21}\right)$ can be obtained:

$$e_a^{21} = \left|\left(\Phi_1 - \Phi_2\right) / \Phi_1\right|, \tag{10}$$

$$e_{ext}^{21} = \left|\left(\Phi_{ext}^{21} - \Phi_1\right) / \Phi_{ext}^{21}\right|. \tag{11}$$

2.2 Turbulence models

In computational fluid mechanics one of the most important decision of the simulation procedure to choose the best turbulence models for the given problem (Kristóf, 2019). The first turbulence models were invented in the 19th century (Celik, 1999). As time passed, a lot of different turbulence models had been invented.

Generally, in vehicle aerodynamics the *k*-*ω* SST turbulence model is used. However, another turbulence model also exists, which also has benefits when a vehicle is investigated with CFD method. This turbulence model is the *k*-*ε* turbulence model.

The basis of the *k*-*ω* SST model is the Wilcox *k*-*ω* model (Ansys, 2019). This model uses model transport equations. The turbulent kinetic energy (k) and the specific dissipation ratio (ω) are calculated from it.

The *k*-*ε* model is a so called two-equation model (Ansys, 2019). This solves two separate transport equations. It also uses two variables: the turbulent kinetic energy (k) as in the case of the *k*-*ω* SST and the dissipation ratio (ε). The specific dissipation ratio can be calculated from the dissipation ratio by dividing it with the turbulent kinetic energy.

As mentioned before, this article investigates two different turbulent models and two different wall treatment methods. In the case of the low Reynolds number wall treatment method, the model uses wall functions to describe the flow near the walls, while in the case of high Reynolds number wall treatment method, the viscous sublayer is resolved (Kristóf, 2019).

3 Structure of the simulation environment

Section 3 includes all the necessary information of the simulations. The CFD simulations were made in ANSYS 2020 R2 (Ansys, online).

3.1 Geometry

The Ahmed body model was created in ANSYS SpaceClaim (Ansys, online). The length of the model is 1044 mm, the height is 288 mm with 50 mm mounting and the width is 389 mm (Lienhart et al., 2000). The detailed size of the geometry is presented in Fig. 1. The model has four mountings which have cylinder shapes. The diameter of the cylinders is 30 mm. For the computational volume sizes, the widely used dimensions were applied (Jackson, 2018). In front of the vehicle 3 car lengths, behind the vehicle 5 car lengths were applied. Beside the vehicle 3 car widths, above it 3 car heights were placed. The dimensions of the computational volume are depicted in Fig. 2.

Three bodies of influence (BOI) were also used during the simulations. The body of influence is a container which helps to control the size of the cells within the volume of the BOI. It can help to get more accurate results and promote the faster convergence. The applied BOIs can be seen in Fig. 3. BOI1 is the biggest one. It involves the whole geometry and the wake after the Ahmed body. BOI2 and BOI3 are placed close to the model. BOI2 is applied for the first part of the model. BOI3 controls the sizes at the end of the body, where the slant angle begins, and it ends after 1 car length. It is important, because right after the vehicle a large separation zone is formed, where the flow is strongly turbulent. This area is difficult to model, so the smoother resolution is required.

3.2 Numerical mesh

The numerical mesh is created with ANSYS Fluent Meshing (Ansys, online). The mesh consists of three main

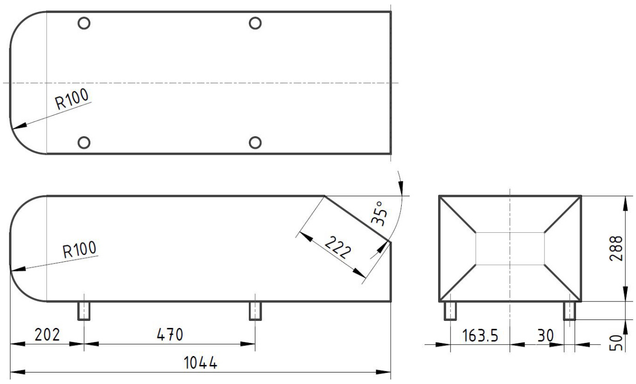

Fig. 1 Sizes of the Ahmed body

Fig. 2 Sizes of the computational volume

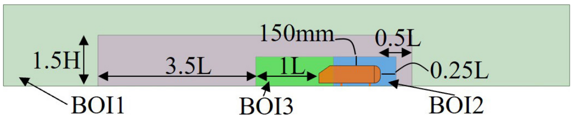

Fig. 3 Sizes of the bodies of influence. BOI1 width is 1.5 W, BOI2 and BOI3 width is 150 mm

parts: the surface mesh, the boundary zone, and the volume mesh. At the surface mesh part, face size, curvature and body of influence cell types were applied. The boundary zone is generated using the last ratio setting. The first layer height of the boundary zone is calculated to get the required y^+ range. Poly-hexcore cells were used for the volume mesh. The structure of the mesh is depicted in Table 1 and the applied named selections in Fig. 4.

3.3 Simulation setup and its boundary conditions

In all simulations half model was used because of the symmetrical behavior of the geometry. The boundary condition for the inlet surface was set as velocity inlet with uniform velocity distribution. The magnitude of the velocity was 40 m/s. The outlet surface was defined as pressure outlet, where the gauge pressure is zero. The ground is defined as moving wall in the x-direction with 40 m/s lateral velocity. The symmetry plane, the lateral and top planes were defined as symmetry. The other surfaces have stationary wall type with no slip condition.

Table 1 Detailed mesh construction

Mesh type	Named selection	Size (mm)	
Face size	Bigger flat parts Curved parts	Target	2.5
	Smaller flat parts Mountings	Target	1.5
Curvature	Curved parts	Minimum	0.5
		Maximum	2.5
	Mountings	Minimum	0.5
		Maximum	1.5
BOI	BOI1	Target	50
	BOI2	Target	12
	BOI3	Target	7
Surface mesh	–	Minimum	0.5
	–	Maximum	75
Volume mesh	–	Maximum	128
Boundary zone		Low Re wall treatment	High Re wall treatment
	First layer height	0.1 mm	7 mm
	Number of layers	10	6
	Cell count	7.38 × 106	4.79 × 106

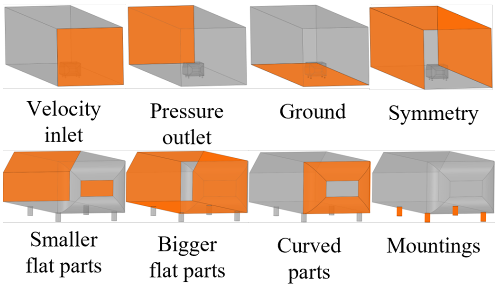
Velocity inlet
Pressure outlet
Ground
Symmetry
Smaller flat parts
Bigger flat parts
Curved parts
Mountings

Fig. 4 Applied named selections

The simulations were made with two different turbulent models: one was the k-ω SST and the other was the k-ε Realizable turbulence model. The k-ε turbulence model was used with the Enhanced wall treatment mode. The material of the fluid was air with constant density $\rho = 1.225$ kg/m^3. The energy equation was turned off.

Coupled scheme was used for the solution method. The spatial discretization was set as Least Squares Cell Based for the gradient, second order for the pressure and second order upwind for the momentum. The turbulent kinetic energy and the specific dissipation rate was defined as first order upwind.

The relaxation factors were used with their default values: pressure and momentum 0.5, density, body forces and turbulent viscosity 1, turbulent kinetic energy and specific dissipation ratio 0.75. The convergence was measured with the drag force and lift force, which were set at the report definition part. The simulation was initialized with hybrid initialization method. The simulations reached the convergence in less than 200 iterations in all cases.

4 Results

4.1 Mesh independence study

In this article the drag force and the lift force were used to examine the meshes. For the investigation the k-ω SST turbulence model with low Reynolds number wall treatment method was used. The mesh sizes were refined by 1.6 uniformly for the fine and coarse meshes. The mesh convergence study was made with the Grid Convergence Index method (GCI). Table 2 contains all the necessary information of the convergence study.

Table 2 Result of the GCI study

	Fine	Medium	Coarse
Cell count	19.2×10^6	7.38×10^6	2.51×10^6
Drag force (N)	33.98	34.69	44.6
Lift force (N)	−5.68	−4.13	36.68
Cell size (h)	3.73×10^{-3}	5.14×10^{-3}	7.36×10^{-3}
Ratio of cell sizes (r_{M-C})	1.38		
Ratio of cell sizes (r_{F-M})	1.43		
	Drag force	Lift force	
Order of convergence (p)	7.26	9.05	
Extrapolated solution $\left(\Phi_{ext}^{M-F}\right)$	33.9 N	−5.77 N	
Relative error $\left(e_a^{M-F}\right)$	2.09%	27.29%	
Extrapolated relative error $\left(e_{ext}^{M-F}\right)$	0.23%	1.59%	

As it can be seen the relative error of the drag force is 2.09%. However, in the case of the lift force, the relative error is bigger (over 25%). This could be caused by the separation zone after the vehicle, where the flow is highly turbulent. With that computational capacity, the lift force and probably the separation zone after the vehicle cannot be modelled properly enough. To visualize the result of the convergence study Richardson plots were created (Kristóf, 2019). These plots are depicted in Figs. 5 and 6.

Based on the relative errors and the Richardson plot the created meshes are of appropriate quality.

4.2 y^+ distribution

Different wall treatment methods have different requirements for the y^+ value. The y^+ value should be between 1 and 10 in the case of low Reynolds number wall treatment and the required y^+ range for the high Reynolds number wall treatment method is between 30 and 300. In Fig. 7 the y^+ distribution is presented for all different cases. As it can be seen the y^+ distribution is almost everywhere in the correct range.

4.3 Comparison of different turbulence models and wall treatment methods

To compare the different turbulent models and wall treatment methods the drag force, the lift force and some flow pictures will be examined.

The drag force and downforce results are compared to experiment results (Meile et al, 2011). As it can be seen in Fig. 8 the drag coefficient results are in the same order with the measured drag coefficient. The lift coefficients differ significantly from the measured one. The reason, as mentioned before in the convergence study section, is that the mesh is not fine enough to describe properly the separation zone after the body.

Fig. 9 shows the relative errors between the different cases in respect of the measured drag coefficient. The results of the k-ε turbulence model have significantly smaller errors than the results from the k-ω model. In the case of k-ε the errors are below 5 percent in both cases, while in the k-ω cases the errors are over than 10%. From wall treatment point of view, high Reynolds number wall treatment methods have smaller errors in both cases.

In Fig. 10 the static pressure distribution is depicted. The flow distribution is very similar at the stagnation point. After it where the flow detached from the edges, the shape of the separation zones and its velocities are the same. However, after the vehicle, where the largest separation zone takes place, the flow distributions differ from each other. In the case of the low Reynolds wall treatment method, bigger separation zone is formed, than in the other cases. Above the slanted surface, the pressure is smaller, so bigger lift force should be generated here.

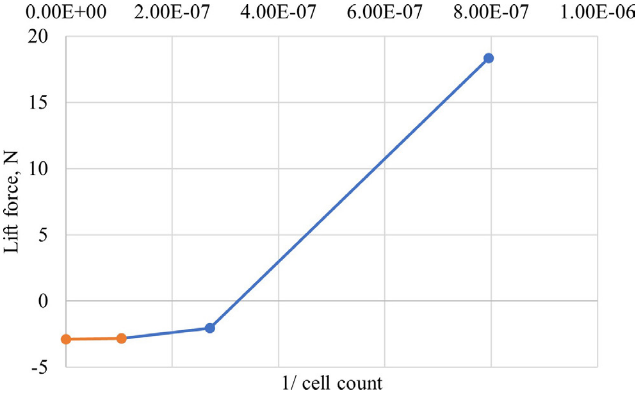

Fig. 5 Richardson plot of the lift force

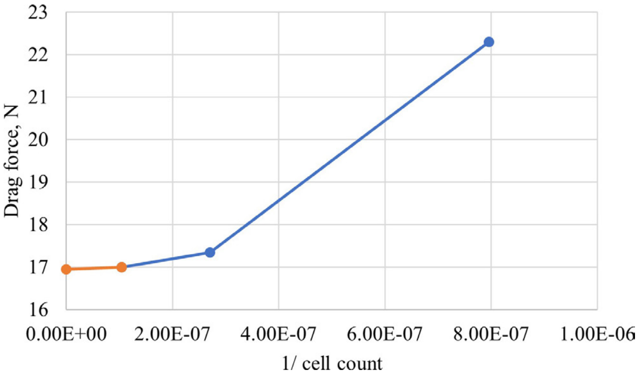

Fig. 6 Richardson plot of the drag force

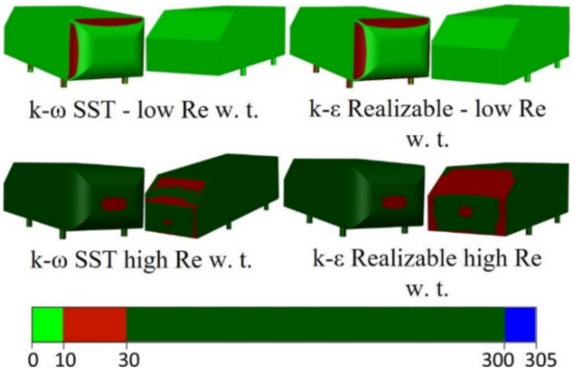

Fig. 7 y^+ distribution for low and high Reynolds number wall treatment methods

The velocity distribution in the main wake zone is depicted in Fig. 11. From the velocity point of view, the wake zones differ less from each other than in the case of the static pressure. The zones are longer and more robust in the case of the low Reynolds wall treatment method which could cause bigger drag force and lift force.

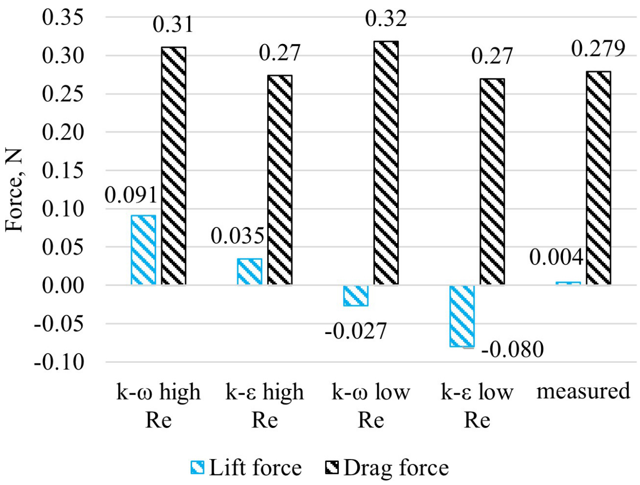

Fig. 8 Numerical results of the drag and lift coefficients in the different cases

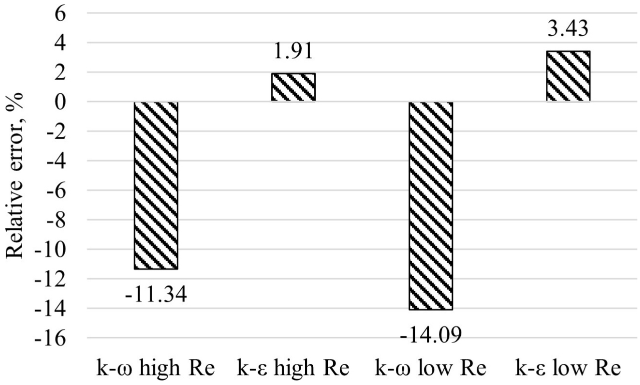

Fig. 9 Relative error distribution of the drag coefficients in respect of the measured results

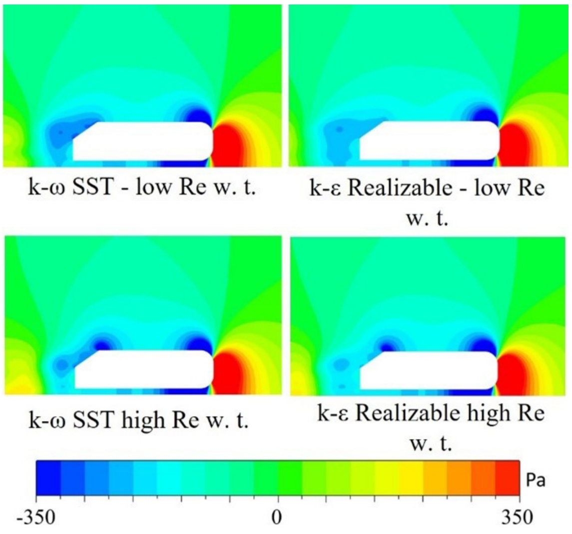
k-ω SST - low Re w. t.
k-ε Realizable - low Re w. t.
k-ω SST high Re w. t.
k-ε Realizable high Re w. t.

Fig. 10 Static pressure distribution close to the Ahmed body in the symmetry plane

For instance, in the case of the *k-ω* low Re wall treatment method, larger drag force can be seen, but in both cases, instead of increased list forces, these are decreased related to Fig. 8. The middle of the zones is more coherent and less disturbed in the case of *k-ε* cases which could cause smaller drag coefficient.

In Fig. 12 the rear surfaces of the Ahmed body are presented with wall shear distribution. Significant differences

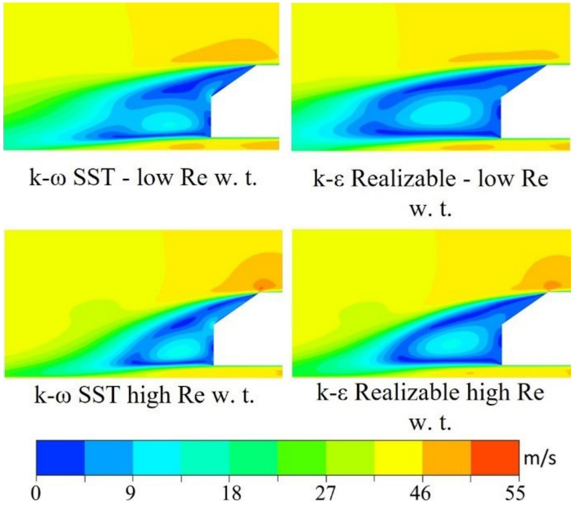
k-ω SST - low Re w. t.
k-ε Realizable - low Re w. t.
k-ω SST high Re w. t.
k-ε Realizable high Re w. t.

Fig. 11 Velocity distribution of the wake zone after the vehicle in the symmetry plane

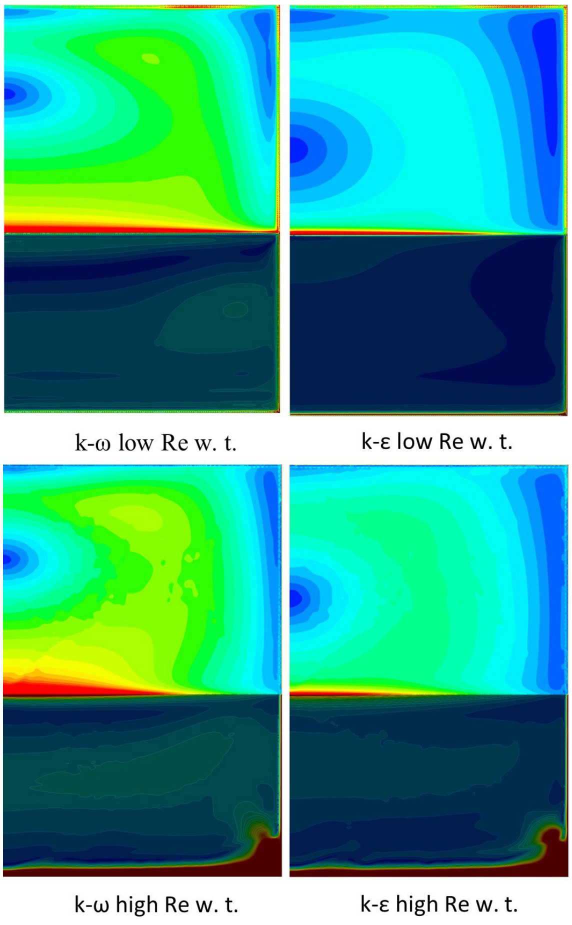
k-ω low Re w. t.
k-ε low Re w. t.
k-ω high Re w. t.
k-ε high Re w. t.

Fig. 12 Wall shear stress distribution from the back view on the rear side of the Ahmed body exist between *k*-*ω* and *k*-*ε* turbulence models. It can be stated that the shear stresses in the case of *k*-*ω* turbulence models are bigger uniformly on the slanted surface. It means that the flow is more detached here. It is also clear that at the bottom rear edge, the shear stress is larger in the case of high Reynolds wall treatment cases. The reason is that the air flow is slower under the body in the case of the high Reynolds wall treatment method so the flow can reattach easier, and it causes larger wall shear stresses there.

5 Conclusion

The turbulence model and wall treatment method examination were carried out successfully. The results were examined in different ways such as numerical results and contour plots.

The *k*-*ε* turbulence model produced more accurate results in several points than the *k*-*ω* turbulence model. The high Reynolds number wall treatment method also gave several times more accurate results than the low Reynolds number wall treatment method. If the high Reynolds wall treatment method can be used instead of the low Reynolds number wall treatment the cell count could be decreased by 35%.

Based on the investigation the optimal turbulence model, wall treatment method pair cannot be chosen yet, further examinations are proposed. More comparison is needed between the result of the CFD simulations and the measured data.

Acknowledgement

The research presented in this paper was carried out as part of the EFOP-3.6.2-16- 2017-00016 project in the framework of the New Széchenyi Plan. The completion of this project is funded by the European Union and co-financed by the European Social Fund.

References

Ansys, Inc. (2019) "ANSYS Fluent Theory Guide", ANSYS Drive, Canonsburg, PA, USA.

Ansys, Inc. "Ansys Fluent, (2020 R2)", [computer program] Available at: www.ansys.com/products/fluids/ansys-fluent [Accessed: 27 May 2023]

Banga, S., Zunaid, M., Ansari, N. A., Sharma, S., Dungriyal, R. S. (2015) "CFD Simulation of Flow around External Vehicle: Ahmed Body", Journal of Mechanical and Civil Engineering (IOSR-JMCE), 12(4), pp. 87–94. https://doi.org/10.9790/1684-1204038794

Bayraktar, I., Landman, D., Baysal, O. (2001) "Experimental and Computational Investigation of Ahmed Body for Ground Vehicle Aerodynamics", SAE Technical Paper, No. 2001-01-2742. https://doi.org/10.4271/2001-01-2742

Bing-xin, W., Zhi-gang, Y., Hui, Z. (2019) "Active flow control on the 25° Ahmed body using a new unsteady jet", International Journal of Heat and Fluid Flow, 79, 108459. https://doi.org/10.1016/j.ijheatfluidflow.2019.108459

Bruneau, C.-H., Gillérion, P., Mortazavi, I. (2007) "Flow manipulation around the Ahmed body with a rear window using passive strategies", Comptes Rendus Mécanique, 335(4), pp. 213–218. https://doi.org/10.1016/j.crme.2007.03.003

Buscariolo, F. F., Assi, G. R. S., Sherwin, S. J. (2021) "Computational study on an Ahmed Body equipped with simplified underbody diffuser", Journal of Wind Engineering and Industrial Aerodynamics, 209, 104411. https://doi.org/10.1016/j.jweia.2020.104411

Celik, I. B. (1999) "Introductory Turbulence Modeling", Mechanical and Aerospace Engineering Department, West Virginia University, Morgantown, WV, USA, Rep. WV 26506-6106.

Celik, I. B., Ghia, U. J. Roache, P. J. Freitas., C., Coleman, H. E., Raad, P. (2008) "Procedure for Estimation and Reporting of Uncertainty Due to Discretization in CFD Applications", Journal of Fluids Engineering, 130(7), 078001. https://doi.org/10.1115/1.2960953

Corallo, M., Sheridan, J., Thompson, M. C. (2015) "Effect of aspect ratio on the near-wake flow structure of an Ahmed body", Journal of Wind Engineering and Industrial Aerodynamics, 147, pp. 95–103. https://doi.org/10.1016/j.jweia.2015.09.006

Delassaux, F., Mortazavi, I., Itam, E., Herbert, V., Ribes C. (2021) "Sensitivity analysis of hybrid methods for the flow around the ahmed body with application to passive control with rounded edges", Computers & Fluids, 214, 104757. https://doi.org/10.1016/j.compfluid.2020.104757

Galipeau-Bélair, P., El-Gindy, M., Ghantae, S., Critchley, D., Ramachandra, S. (2013) "A review of side underride statistics and protection device literature and designs", International Journal of Heavy Vehicle Systems, 20(4), pp. 361–374. https://doi.org/10.1504/IJHVS.2013.056813

Hucho, W.-H. (1987) "Aerodynamics of Road Vehicles: From Fluid Mechanics to Vehicle Engineering", Butterworth-Heinemann. ISBN 978-0-7506-1267-8 https://doi.org/10.1016/C2013-0-01227-3

Jackson, F. (2018) "Aerodynamic optimization of Formula student vehicle using computational", Fields: Journal of Huddersfield Student Research, 4(1). https://doi.org/10.5920/fields.2018.02

Jéger, C., Veress, Á. (2019) "Novell Application of CFD for Rocket Engine Nozzle Optimization", Periodica Polytechnica Transportation Engineering, 47(2), pp. 131–135. https://doi.org/10.3311/PPtr.11490

Kristóf, G. (2019) "Áramlások numerikus modellezése" (Computational Fluid Dynamics), Akadémia Kiadó. ISBN 978 963 454 412 8 https://doi.org/10.1556/9789634544128

Lienhart, H., Becker, S., Stoots, C. (2000) "Flow around a simplified car body (Ahmed body)", Classic Collection Database, [online] Available at: http://cfd.mace.manchester.ac.uk/ercoftac/doku.php?id=cases:case082 [Accessed: 15 April 2023]

Matijošius, J., Juciūtė, A., Rimkus, A., Zaranka, J. (2022) "Investigation of the Concentration of Particles Generated by Public Transport Gas (CNG) Buses", Cognitive Sustainability, 1(1). https://doi.org/10.55343/cogsust.10

Meile, W., Brenn, G., Reppenhagen, A., Lechner, B., Fuchs, A. (2011) "Experiments and numerical simulations on the aerodynamics of the Ahmed body", CFD Letters, 3(1), pp. 32–39. [online] Available at: https://www.researchgate.net/publication/330383775_Experiments_and_numerical_simulations_on_the_aerodynamics_of_the_Ahmed_body [Accessed: 10 April 2023]

Minguez, M., Pasquetti, R., Serre, E. (2008) "High-order large-eddy simulation of flow over the "Ahmed body" car model", Physics of Fluids, 20(9), 095101. https://doi.org/10.1063/1.2952595

Ragheb, H., El-Gindy, M. (2022) "Rear wing spoiler effects on vehicle stability and aerodynamic performance", International Journal of Vehicle Systems Modelling and Testing, 15(4), pp. 289–307. https://doi.org/10.1504/IJVSMT.2021.122817

Rao, A., Minelli, G., Basara, B., Krajnović, S. (2018) "On the two flow states in the wake of a hatchback Ahmed body", Journal of Wind Engineering and Industrial Aerodynamics, 173, pp. 262–278. https://doi.org/10.1016/j.jweia.2017.10.021

Suda, J. M. (2022) "Vehicle Aerodynamics Part III. - History", Department of Fluid Mechanics, Budapest University of Technology and Economics, Budapest, Hungary.

Székely, P., Ficzere, F. (2017) "The Examination of Dynamic Effects of Shape Optimized Vehicle Components", Periodica Polytechnica Transportation Engineering, 45(2), pp. 90–93. https://doi.org/10.3311/PPtr.9875

Tunay, T., Sahin, B., Ozbolat, V. (2014) "Effects of rear slant angles on the flow characteristics of Ahmed body", Experimental Thermal and Fluid Science, 57, pp. 165–176. https://doi.org/10.1016/j.expthermflusci.2014.04.016

Venning, J., McQueen, T., Jacono, D. L., Burton, D., Thompson, M., Sheridan, J. (2022) "Aspect ratio and the dynamic wake of the Ahmed body", Experimental Thermal and Fluid Science, 130, 110457. https://doi.org/10.1016/j.expthermflusci.2021.110457

Veress, Á., Molnár, J., Rohács, J. (2008) "Compressible viscous flow solver", Periodica Polytechnica Transportation Engineering, 37(1–2), pp. 77–81. https://doi.org/10.3311/pp.tr.2009-1-2.13

Vučetić, A., Sraga, V., Bućan, B., Ormuž, K., Šagi, G., Ilinčić, P., Lulić, Z. (2022) "Real Driving Emission from Vehicle Fuelled by Petrol and Liquefied Petroleum Gas (LPG)", Cognitive Sustainability, 1(4). https://doi.org/10.55343/cogsust.38

Wei, Y. (2017) "The development and application of CFD technology in mechanical engineering", IOP Conference Series: Materials Science and Engineering, 274, 012012. https://doi.org/10.1088/1757-899X/274/1/012012